Leveraging isotopologues as a general strategy to image neurotransmitters with vibrational microscopy.

Gabriel F. Dorlhiac[1], Markita P. Landry[1,2,3,4,5*], Aaron Streets[1,4,5,6,7*]

[1]Biophysics Graduate Group, University of California Berkeley, Berkeley, CA, 94720, USA
[2]Department of Chemical and Biomolecular Engineering, University of California, Berkeley, Berkeley, CA, 94720, USA
[3]Innovative Geneomics Institute, University of California Berkeley, Berkeley, CA, 94720, USA
[4]California Institute for Quantitative Biosciences, QB3, University of California, Berkeley, Berkeley, CA, 94720, USA
[5]Chan-Zuckerberg Biohub, San Francisco, CA, 94158, USA
[6]Department of Bioengineering, University of California, Berkeley, Berkeley, CA, 94720, USA
[7]UC Berkeley-UC San Francisco Graduate Program in Bioengineering, University of California, Berkeley, Berkeley, CA, 94720, USA

Abstract

Chemical neurotransmission is central to neurotypical brain function but also implicated in a variety of psychiatric and neurodegenerative diseases. The release dynamics of neurotransmitters is correlated with but distinct from electrical signal propagation. It is therefore necessary to track neurotransmitter modulation separately from electrical activity. Here, we present a new approach for imaging deuterated neurotransmitter molecules with vibrational microscopy in the cell-silent window. Using stimulated Raman scattering microscopy, we perform direct imaging of the neurotransmitters dopamine and GABA in PC12 chromafin cells, and primary hippocampal neurons, respectively, based on their C-D vibrational frequencies. We find that isotope labelling does not perturb neurochemical activity. We further show that stimulation of neurotransmitter release results in an overall 20-50% signal reduction, with the ability to observe inter- and intracellular variation in vesicular release potential. Taken together, our data suggest that neurotransmitter isotopologues can serve as a generic, non-perturbative, method to image neurotransmitters.

Introduction

Information flow in the nervous system is mediated by both electrical and chemical transmission processes, an understanding of both of which is necessary to study neurotypical activity, and any deviations which can result in neuropathology. Neuronal stimulation results in intracellular electrical signal propagation, in the form of action potentials, on the millisecond timescale. Interneuronal communication, however, is most often mediated by small molecule, i.e. neurotransmitter, release at the neuronal synapse. Canonically these neurotransmitters are locally confined to the sub-micron sized synapse, leading to rapid com-

munication shortly following action potential arrival. One class of neurotransmitters, known as neuromodulators, are thought to exhibit additional extrasynaptic diffusive action, which may modulate broader neuronal networks on the order of microns and seconds. Frequently, the release of these compounds is also not well correlated with action potential arrival, as in the case of dopamine, where estimates of the correlation are as low as 6-10% (1, 2). Abnormal regulation of neuromodulator activity is associated with a wide variety of neuropathologies, including schizophrenia (3), epilepsy (4), Parkinson's (5), and Huntington's disease (6), and addiction (7), among others. The study of chemical neurotransmission is, therefore, of fundamental importance to our understanding of neuropathologies.

Owing to the high spatiotemporal resolution of fluorescence imaging, its adaptability to image whole organs and organisms, and the broad abundance of fluorescence-based probes to image neurons and neuronal activity, fluorescence-based techniques have been widely adopted to study the brain and the process of neurotransmission.

However, fluorescence-based approaches face a major obstacle when imaging neurochemical communication, in that neurotransmitters are small molecules that do not intrinsically fluoresce in the visible range. Therefore, several approaches have been taken to enable fluorescence-based measurements of neurotransmitter activity, including synthesis of fluorescent chemical analogues, the use of genetically encoded receptors with affinity for the neurotransmitter of interest, and readout of neuron activity by fluorescent reporters as a proxy for neurotransmitter release. For instance, monitoring of vesicular fusion can be accomplished through introduction of exogenous amphipathic FM dyes (8), or by using the acidic vesicular environment to quench genetically encoded pHluorin sensors (9), which report on fusion when exposed to the neutral synaptic environment. Yet neither technique reports on the neurotransmitter populations themselves inside the vesicles, nor whether they are released. Other genetically encoded fluorescent receptors report binding of the neurotransmitter itself. For example, cell-based neurotransmitter fluorescent engineered reporters (CNiFERS), linking neurotransmitter-binding G-protein coupled receptors to fluorescent readout, have been used to study a number of different neurotransmitters (10, 11). This technique, however, requires the transplantation of reporter cells into neuronal tissue, exhibiting low spatiotemporal resolution relative to neurochemical signaling. To address this issue GRABDA was developed by engineering dopamine receptors with circularly permuted eGFP, to be expressed in cell membranes, and is used to image exocytosed volume transmission of dopamine (12). Patriarchi et al concurrently produced a suite of genetic encoded sensors, operating on similar principles, called dLight (13). Both probes require extensive protein engineering which is not easily translated to other neurotransmitters, and can only measure neurotransmitters post-exocytosis. Another class of sensors based on near-infrared fluorescent nanoparticles (14)can be localized to the extracellular space in the brain and produce fluorescence changes upon neurotransmitter binding, allowing imaging of synaptic-scale neurotransmitter volume transmission (15). These sensors have recently been used to image dopamine release from somatodendritic processes and to characterize dopamine release from individual synapses (16). All aforementioned fluorescence-based probes face similar research and development challenges, requiring new approaches to their design, development, and deployment with each new neurotransmitter target. Furthermore, their use is limited to the measurement of extracellular analytes, making it difficult to study neurotransmitters in the intracellular environment.

To address the challenge of intracellular neurotransmitter imaging, direct chemical modification of neurotransmitters has been used to produce visible fluorescence, allowing tracking of the molecule itself. False neurotransmitters analogs have been under development for many years as artificial alternatives to their endogenous counterparts. To this end, fluorescent false neurotransmitters (FFN) enable intracellular tracking and subsequent release of the neuromodulators dopamine (17, 18)and serotonin (19). However, relatively large structural changes to the native neurotransmitter are necessary to produce a visibly fluorescent analog, requiring extensive validation and complex syntheses. Furthermore, it remains unclear to what extent the structural modifications present in FFNs affects their biodstribution and function. A number of investigations have therefore used the natural autofluorescence of certain neurotransmitters, such as dopamine and serotonin (20–22). While this approach provides a direct readout of the compound, the use of UV fluorescence limits penetration depth, and limits application to other neurotransmitters.

Fluorescence, however, is not the only physical property that can be used to gain chemical specificity. Molecular vibrations are specific to the types of atoms and bonds in a molecule, and can be probed through a number of different optical interactions, many of which are well suited to implementation as imaging techniques. The most common probes of molecular vibrations are infrared (IR) and Raman spectroscopy, although many others exist including surface-enhanced Raman scattering (SERS), photoacoustic imaging, and nonlinear techniques such as coherent anti-Stokes Raman scattering (CARS), and stimulated Raman scattering (SRS). However, vibrational imaging faces its own difficulty in isolating the vibrational signature of a single molecule of interest in situ in a biological system. A typical vibrational spectrum of a cell contains a substantial amount of information about cellular composition but, even with high spectral resolution, is too complex to deconvolve into individual molecular contributions. To date, only a single neurotransmitter, acetylcholine, has been imaged using vibrational microscopy in the frog neuromuscular junction (23). The lack of subsequent development of vibrational probes for neuroscience illustrates the challenge in specifically imaging a single type of molecule in a complex cellular context.

Nonetheless, in the animal systems of interest, a gap appears in the vibrational spectrum from about 1800 - 2800 cm^{-1}, often called the cell-silent window. This corresponds to the frequency range of alkyne and nitrile vibrations, functional groups that are largely absent from biomoleules in animals. By modifying molecules to have vibrational frequencies in this window, it is possible to image their biodistribution with minimal background from other cellular components. One could directly introduce a triple bond to produce this effect. This strategy has been used to study a number of processes including imaging of newly synthesized DNA by incorporation of 5-ethynyl-deoxyuridine (EdU) (24, 25), to study mitochondria (26), membrane proteins (27), and drug uptake (25, 28). Such a modification was recently proposed to study dopamine; however, imaging based on the alkyne vibration has not yet been demonstrated (29).
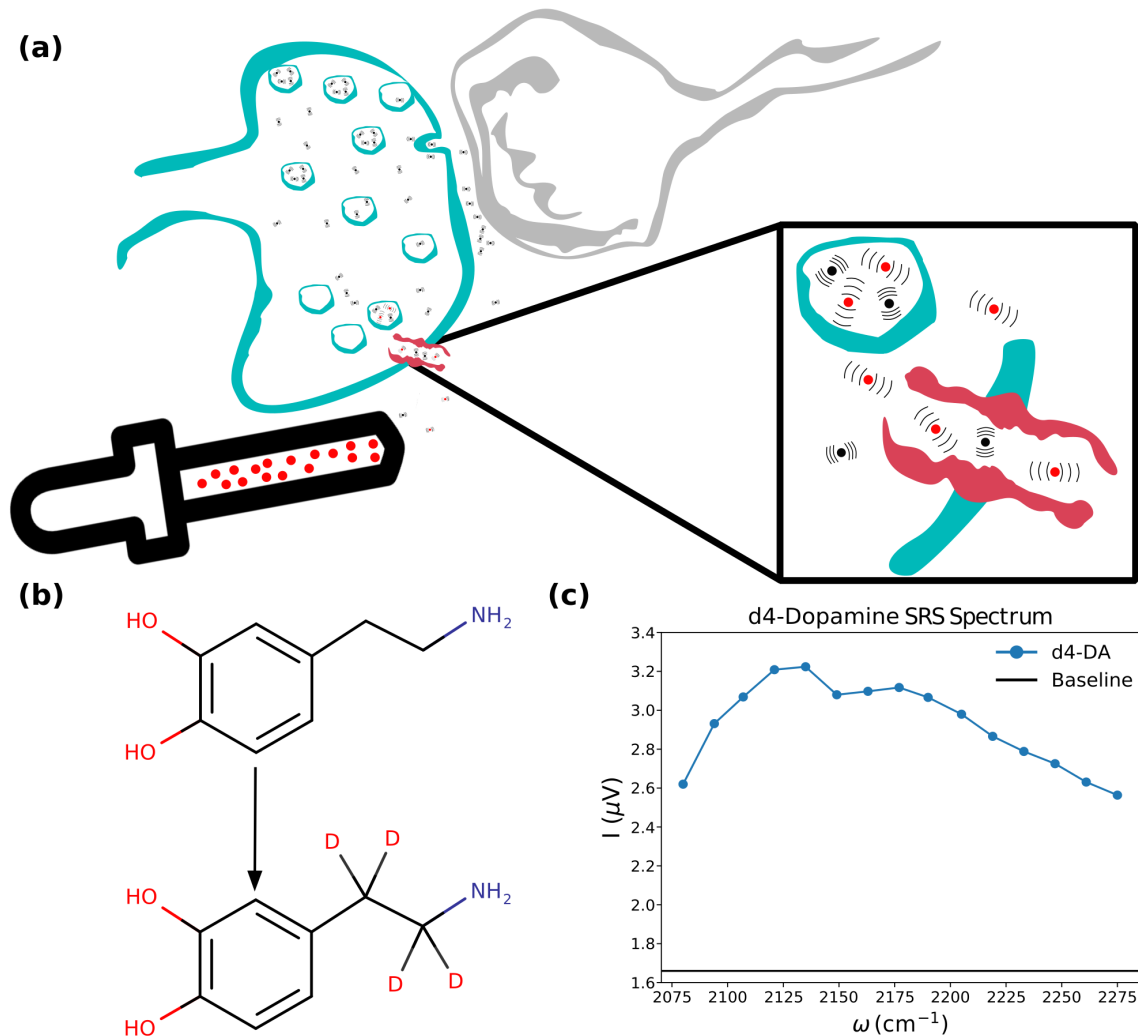
Fig. 1 Overview of isotopologue imaging with vibrational microscopy.
(a) Deuterated neurotransmitters are incubated with the sample of interest. Endogenous neurotransmitter transporters uptake the deuterated isotopologues, facilitating their packaging into vesicles and allowing their visualization using vibrational microscopy techniques such as stimulated Raman scattering (SRS). (b) The commercially available, four deuterium substituted dopamine isotopologue used for tracking dopamine uptake and release. (c) The SRS spectrum of the dopamine isotopologue.

An alternative strategy to the incorporation of alkyne functional groups is to use isotope labeling, as the frequency of a molecular vibration is inversely proportional to the reduced mass of the atoms involved. Increasing the mass of the involved atoms will therefore reduce the vibrational frequency, for example by employing one of two common isotopic substitutions used in mass spectrometry and nuclear magnetic resonance (NMR): ^{1}H to ^{2}H (D) or 12C to 13C. These substitutions move the C-H stretches that are normally at 2800-3000 cm^{-1} down into the cell-silent window. Isotope labeled compounds have been used in con-

4

jugation with vibrational imaging to study lipid and cholesterol dynamics (30), proteome degradation in steady-state as well as with Huntington protein aggregation (31), in addition to being used as a general readout of metabolic activity (32). Furthermore, due to the application of isotope labeling in mass spectrometry and NMR, many neurotransmitters are already commercially available in isotope-labeled form, as analytical standards. This availability provides a rapid source of neurotransmitters with vibrational signatures that can be easily separated from the cellular background, obviating the need for special syntheses, or genetic engineering. We hypothesize these compounds can be introduced into neurobiological systems or cell cultures, and uptaken by endogenous neurotransmitter transporters (Figure 1a), where vesicular populations of the neurotransmitter of interest can then be monitored under native conditions.

In this report, we demonstrate the application of SRS microscopy with this labeling strategy to image two such commercially-available deuterated neurotransmitters, d_4-dopamine (d_4-DA) and d_6-γ-aminobutyric acid (d_6-GABA), in cultured PC12 cells and primary hippocampal neurons, respectively. SRS is a coherent 3rd order nonlinear process which makes use of two pulsed lasers, and is implemented in a point-scanning configuration for microscopy, like with multiphoton excited fluorescence microscopy. The two laser frequencies are chosen such that the difference in their frequency is resonant with a vibrational mode of interest. As such, for any single image only a single spectral channel is acquired, in contrast to confocal spontaneous Raman microscopy. However, through coherent driving of the vibration, signal enhancements of up to 108 over spontaneous Raman scattering can be obtained (33, 34). We show that leveraging this signal enhancement allows for visualization of d_4-DA and d_6-GABA neurotransmitter isotopologues at speeds comparable to confocal fluorescence microscopy, with probe structures that are functionally identical to their native counterparts.

Results

SRS microscopy allows observation of uptake and release of d_4-DA

As a proof of principle we investigated the capability to image the uptake and intracellular distribution of d_4-DA in cultured PC12 cells. The PC12 cell line, derived from rat chromaffin cells in the 1970s, is a popular in vitro culture system for studying catecholamines and neurite development (35). Figure 1b shows the hydrogen-to-deuterium substitutions made for this particular isotopologue, while its corresponding SRS spectrum acquired in the cell-silent window is displayed in panel c. We first tested the ability to detect uptake of the labeled compound d_4-DA, by adding it to a final concentration of 50 μM to the cell culture medium. The PC12 cells were incubated for one hour, after which they were washed and then imaged in a PBS buffer.

To verify uptake, images were acquired at 2135 cm^{-1}, the maximum of the d_4-DA spectrum in this window (figure 1c), and compared to the images of cells which were not pre-incubated with the compound. To provide a reference for the location and structure of the entire cell, images were also acquired at 2950 cm^{-1}, corresponding to CH3 stretches, a signal largely dominated by proteins. d_4-DA internalization was observed for the d_4-DA-incubated cells, largely localized to the cell periphery, and in punctate structures, with clear nuclear

exclusion (figure 2a, middle row). Under identical imaging and culture conditions, unincubated cells displayed no such signal, consistent with detection of a signal specific to the d_4-DA neurotransmitter (figure 2a, top row). We observe a significant separation between the average intracellular signal intensity in incubated vs unincubated cells (figure 3a; p < 0.001, $\Delta > 15$).
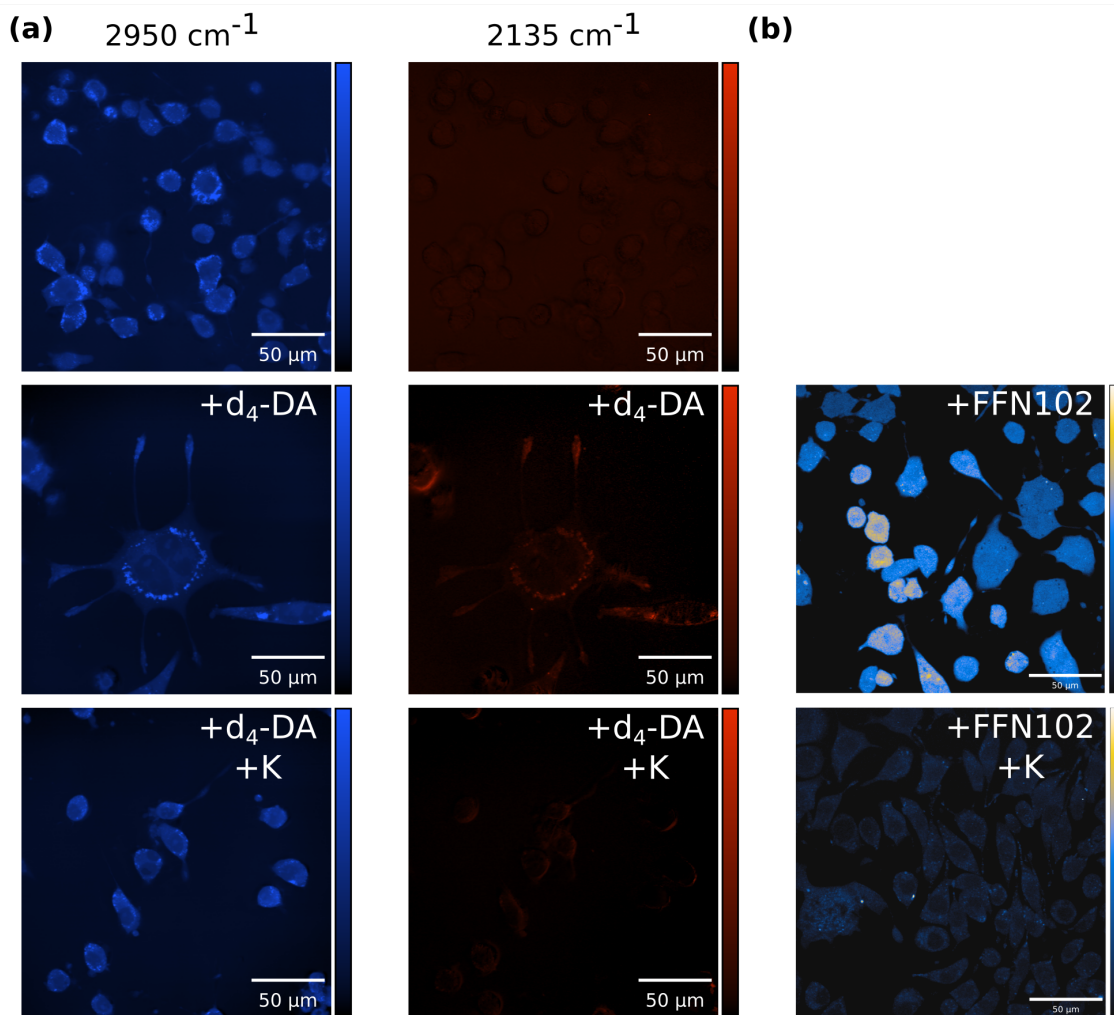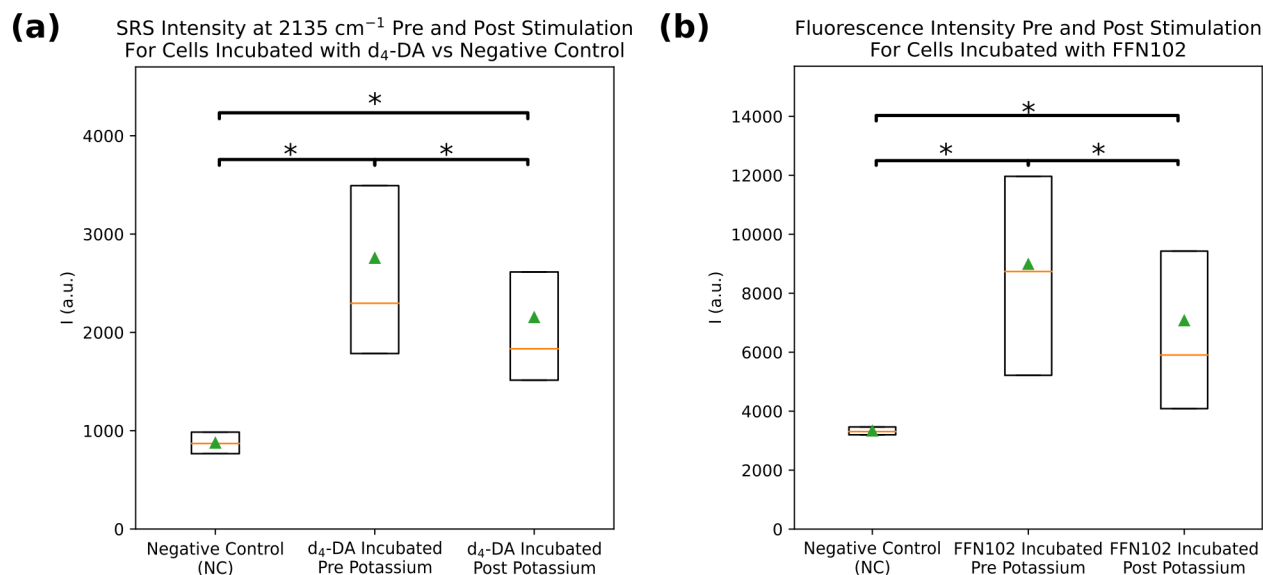

Fig. 2 SRS and two-photon fluorescence imaging of a deuterated dopamine isotopologue and a false fluorescent analogue in PC12 cells.

(a) SRS images of PC12 cells without incubation with the deuterated dopamine isotopologue (top), with incubation with the dopamine isotopologue (middle), and with incubation with the dopamine isotopologue, but two minutes post stimulation to release neurotransmitter with 50 mM potassium (bottom). The left column displays images at 2950 cm-1, the C-H stretching frequency range, broadly corresponding to protein signal and allowing cell localization. The right column displays images at 2135 cm-1, the C-D stretching frequency range, corresponding to the signal originating from the deuterated dopamine compound. (b) Two-photon excited fluorescence images of PC12 cells incubated with a false fluorescent neurotransmitter, FFN102 (top), and cells incubated with

FFN102 imaged two minutes post stimulation to release neurotransmitter with 50 mM potassium.

The observed subcellular distribution of d_4-DA reveals signal along the cell periphery and in distinct puncta as predicted, suggesting a biologically-relevant internalization mechanism, with the isotopologue confined to intracellular vesicles. Comparatively little to no signal is observed outside these bright puncta, consistent with a much lower concentration of neurotransmitter present in the cytoplasm, estimated to be $0.5 - 5$ μM (36, 37), compared to $110 - 190$ mM in the vesicles (38, 39). Furthermore, we observe the expected lack of internalization into the nucleus. To test whether this d_4-DA signal did arise from an active vesicular population of d_4-DA, we repeated the incubation experiments, stimulated d_4-DA release with 50 mM potassium, and imaged cells two minutes post-stimulation. In line with the expected response to potassium stimulation, there was an observable decrease in the measured d_4-DA signal for the population of cells imaged post stimulation (figure 2a, bottom row), which is significant compared to the unstimulated cells (figure 3a; $p < 0.001$, $\Delta > 0.35$). This 22% decrease is commensurate with prior reports that quantal release of dopamine in PC12 cells is fractional.

We compared the response to potassium stimulation in PC12 cells incubated with d_4-DA to PC12 cells incubated with a dopamine FFN, FFN102 ([FFN102]=10 μM). A strong signal was visible within cells incubated with the fluorescent analogue when imaged by two-photon excited fluorescence (TPEF) microscopy (figure 2b, middle row). Notably, there was stronger readout from the entire cell, perhaps due to the higher sensitivity of TPEF to measure lower cytoplasmic concentrations of the analogue; however, unlike d_4-DA-labeled cells, some FFN signal was observed in the nucleus suggesting some non-specific internalization mechanisms of the dopamine FFN analogue. FFN102-incubated cells imaged post potassium stimulation also displayed a lower overall signal (figure 2b, bottom row). This 21% decrease for FFN-incubated cells post stimulation was observed to be significant over a large sample of cells (figure 3b; $p < 0.001$, $\Delta > 0.48$). The two distributions for d_4-DA and FFN102, in fact, show very similar trends, and suggest d_4-DA can report on relevant dopamine uptake and release in cultured cells.

(a) SRS Intensity at 2135 cm^{-1} Pre and Post Stimulation For Cells Incubated with d$_4$-DA vs Negative Control

(b) Fluorescence Intensity Pre and Post Stimulation For Cells Incubated with FFN102

Fig. 3 Cell-averaged SRS or fluorescence intensity distributions for cells incubated with deuterated dopamine analogue, or FFN102.

(a) The cell-averaged SRS intensity for cells that were not incubated with deuterated dopamine (left column), cells that were incubated with deuterated dopamine (middle column), and cells that were incubated with deuterated dopamine, stimulated to release neurotransmitter with 50 mM potassium, and imaged two minutes later (right column). * p < 0.001, $\Delta > 15$ (incubated vs negative control), $\Delta > 0.35$ (incubated vs incubated post stimulation). N(negative control) = 1273, N(Incubated, pre-stimulation) = 1152, N(Incubated, post-stimulation) = 1145. (b) The cell-averaged two-photon excited fluorescence intensity for cells that were not incubated with FFN102 (left column), cells that were incubated with FFN102 (middle column), and cells that were incubated with FFN102, stimulated to release neurotransmitter with 50 mM potassium, and imaged two minutes later (right column). *p < 0.001, $\Delta > 0.48$ (incubated vs incubated post-stimulation). N(Negative control) = 1802, N(Incubated, pre-stimulation) = 1904, N(Incubated, post-stimulation) = 2920.

PC12 cells display cell-to-cell heterogeneity of d$_4$-DA uptake and release

We next sought to take pre- and post-stimulation measurements on individual unincubated, d$_4$-DA-incubated, and FFN102-incubated cells. While population level measurements have relevance for several important biological questions, they often obscure cell-to-cell heterogeneity. It is, therefore, frequently of interest to make repeat measurements on the same individual cells. Single-cell measurements are particular relevance for neurons, where measuring the effect of stimulation and the relevant kinetics of neurotransmitter release are of fundamental importance to understand neuro-communication. Furthermore, in PC12 cells,

8

it is known that multiple vesicular populations (40)can exist heterogeneously across individual cells, producing cell-to-cell variability in dopamine concentration that is often not apparent when making bulk population level measurements (35).

To measure d_4-DA concentration within the same PC12 cells pre- and post-stimulation, we built a simple microfluidic flow cell, with inlets for the injection of stimulating potassium solution. Cells were grown inside these devices, composed of coverslips on the top and bottom, and PDMS around the sides.

(a)

(b)

(c)
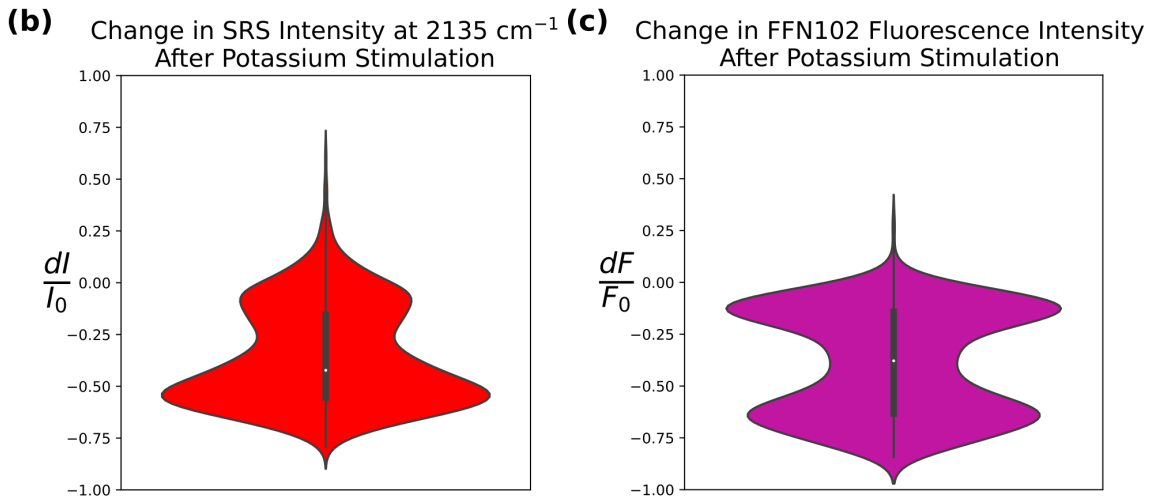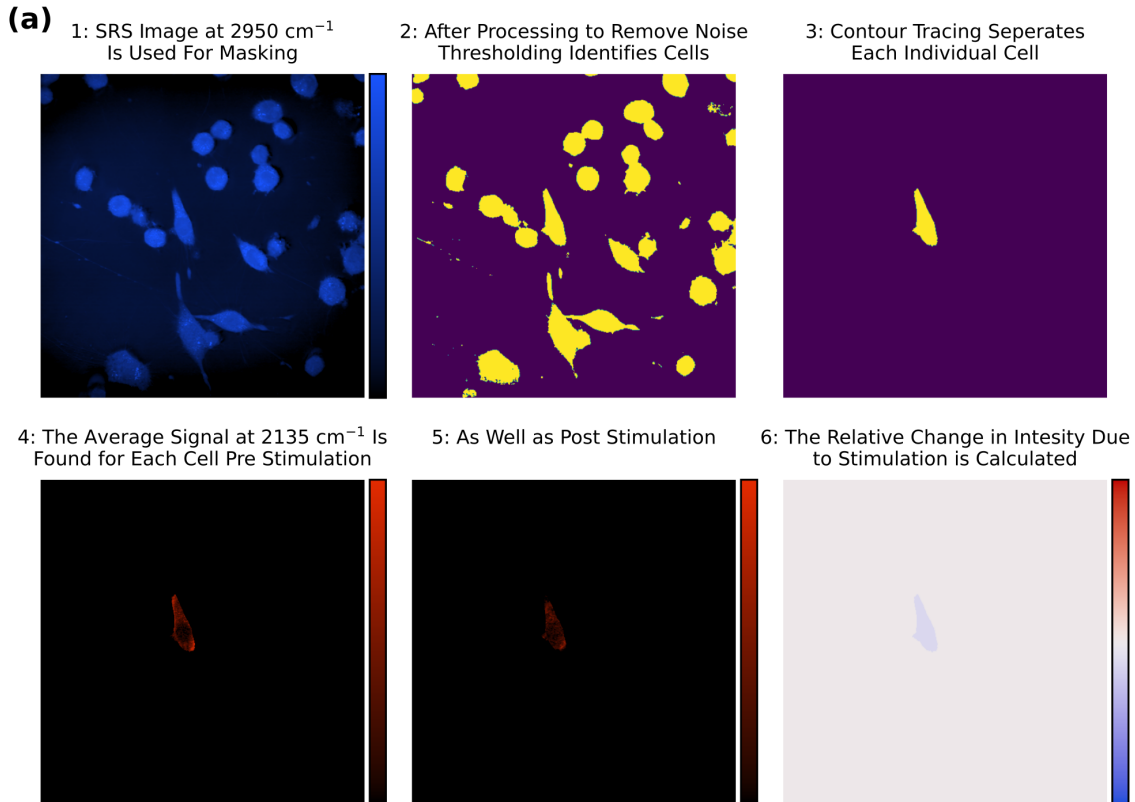
Fig. 4 SRS and two-photon excited fluorescence imaging on the same single cells pre- and post-

9

potassium stimulation.

(a) Workflow for calculation of relative SRS intensity changes due to potassium stimulation. 1. A single image is acquired in the 2950 cm-1 (C-H) channel, broadly corresponding to protein distribution, which is used as a mask. 2. A mask is created from this image using adaptive thresholding and binarization. 3. Contour tracing allows single cells to be retrieved from the mask. 4. A single image is acquired in the 2135 cm-1 (C-D) channel, corresponding to the deuterated dopamine signal. The average signal is determined for each masked cell. 5. The cells are stimulated to release neurotransmitter with 50 mM potassium solution, and a second image in the 2135 cm-1 channel is acquired two minutes later. 6. The relative change in SRS signal is calculated for each masked cell. (b) The distribution of relative SRS intensity change in the 2135 cm-1 channel on a cell-averaged level due to stimulation with 50 mM potassium. (c) The relative change in FFN102 fluorescence intensity due to stimulation with 50 mM potassium.

Using these flow cells, we first incubated PC12 cells with 50 μM d_4-DA, as previously. Prior to imaging the cells were again rinsed; however, imaging was performed in clean culture medium as opposed to PBS. We next acquired acquired an image at 2950 cm^{-1}, to localize cell boundaries, and which served as a mask to identify and separate cells computationally. Subsequently an image was acquired in the 2135 cm^{-1} to quantify d_4-DA concentration prior to stimulation. Next the cells were stimulated to release the isotopologue by exposure to a 50 mM potassium solution, before a second image was acquired at 2135 cm^{-1} to quantify d_4-DA concentration post stimulation (figure 4a). We next quantified the relative change in d_4-DA intensity, i.e. the change in d_4-DA intensity normalized to the initial intensity, in response to potassium stimulation. This analysis revealed a bimodal distribution for PC12 cells incubated with d_4-DA, with one population exhibiting a strong 64% release of d_4-DA in response to potassium stimulation, and another population exhibiting a weaker 15% release of d_4-DA (figure 4b). This bimodal distribution is similar to the distribution observed when the experiment is repeated for PC12 cells incubated with FFN102. We next compared the relative change in intensity due to potassium stimulation versus the initial pre-stimulation intensity in d_4-DA incubated cells (figure S1). We observed a general trend where the greater the initial pre-stimulation intensity, the greater the relative change in intensity in response to potassium stimulation, which was split roughly into two populations. Interestingly, while we observe these two populations for FFN102-incubated cells, a third, high initial intensity, but weakly-responsive, population is also present in FFN102-incubated cell. This result may potentially point to an additional, non-specific, internalization mechanism of the FFN, that is not active for d_4-DA uptake.

d_6-GABA uptake is also observable with SRS microscopy

(a)

(b) d6-GABA SRS Spectrum

I (μV) vs ω (cm^{-1})
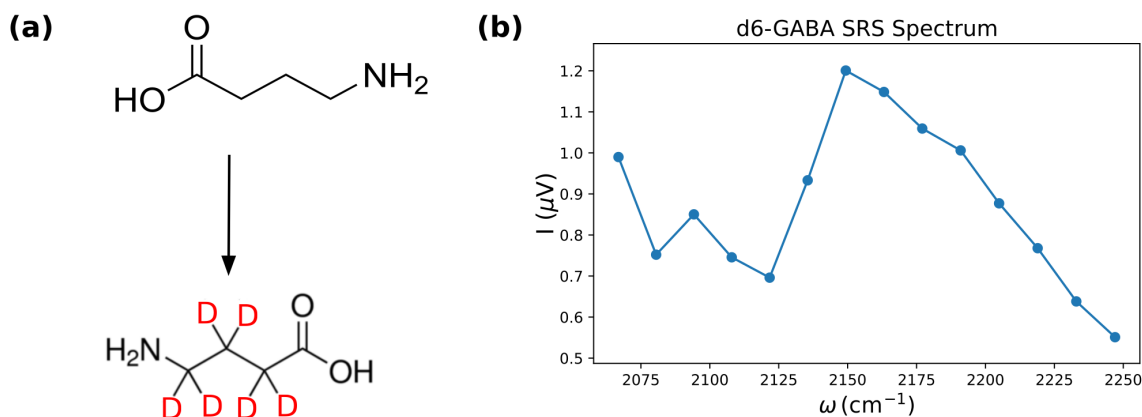
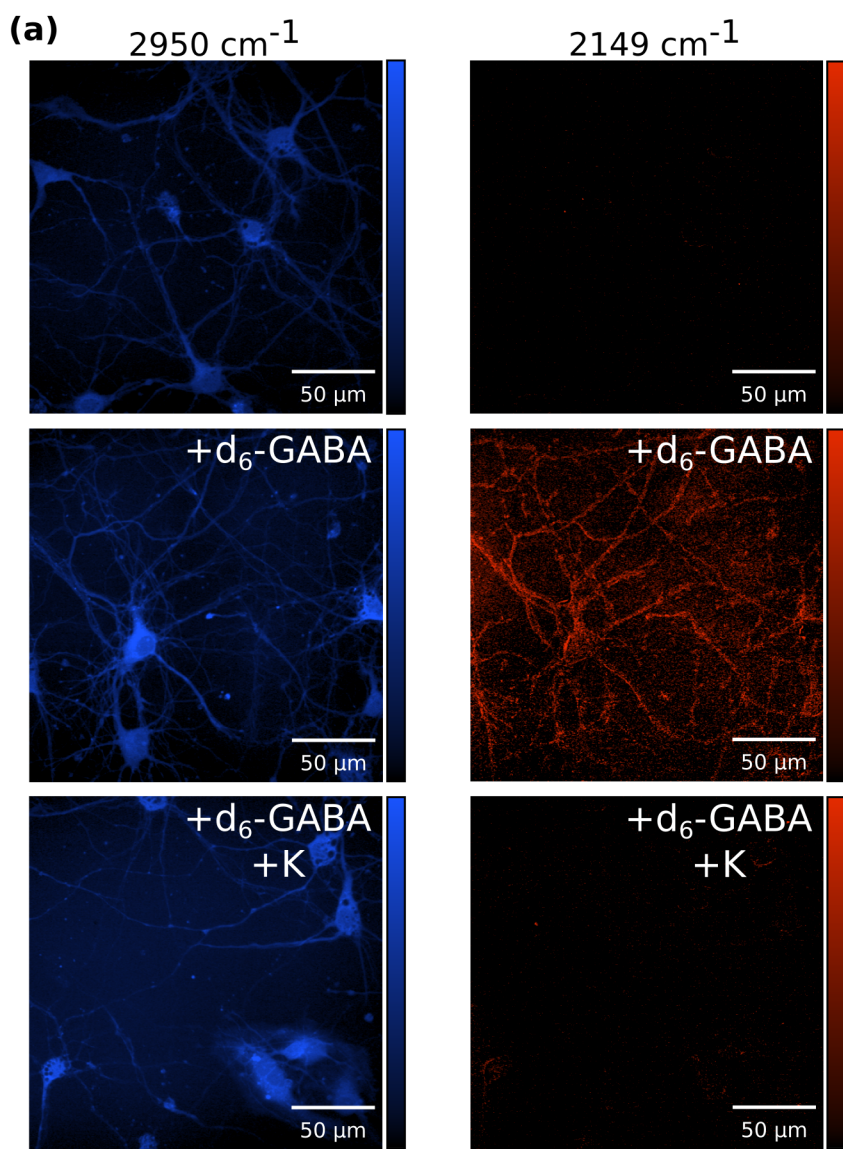**Fig. 5** A deuterated GABA isotopologue and its spectrum.
(a) The H to D substitutions for the commercially available GABA isotopologue used in this study.
(b) The corresponding SRS spectrum for the deuterated GABA istopologue in the cell-silent window.

We next assessed whether the strategy of deuteration and SRS microscopy could be applied more broadly to different commercially-available deuterated neurotransmitters. GABA plays a crucial role in the nervous system as the main inhibitory neurotransmitter, and is consequently centrally implicated in many neurochemical processes throughout the brain. Furthermore, while dopamine as a neuromodulator exhibits volume transmission-based activity, GABA is thought not to, representing a class of neurotransmitter putatively confined to the neuronal synapse. While recent advances have been made for imaging GABA with exogenous fluorophores in FRET-based biosensors (41, 42), and a genetically-encoded GABA biosensor (43), comparatively few tools have been developed for GABA imaging. To test the capability of SRS microscopy to image the uptake and stimulated release of a deuterated GABA isotopologue we used dissociated fetal hippocampal neurons from rat.

The isotopologue used, d_6-GABA, was fully substituted for deuterium at all available carbon bonded hydrogens (figure 5a). Fetal hippocampal neurons, dissociated from day 19 Sprague Dawley rat embryos, were incubated to a final concentration of 50 μM d_6-GABA prior to imaging. d_6-GABA has a different spectral signature in the cell-silent window, so images were acquired instead at the new d_6-GABA maximum of 2149 cm^{-1} (figure 5b) for its visualization. Images were again acquired in the 2950 cm^{-1} channel to provide contrast of the cell body.

Hippocampal neurons displayed a strong signal at 2149 cm^{-1} when incubated with the deuterated neurotransmitter (figure 6, middle row). In contrast to d_4-DA, signal was visible across the entire cell. This whole-cell d_6-GABA biodistribution may be explained by the higher cytoplasmic concentration of GABA, compared to dopamine, which is maintained in the 5 mM range (44, 45). d_6-GABA signal was absent from images acquired from
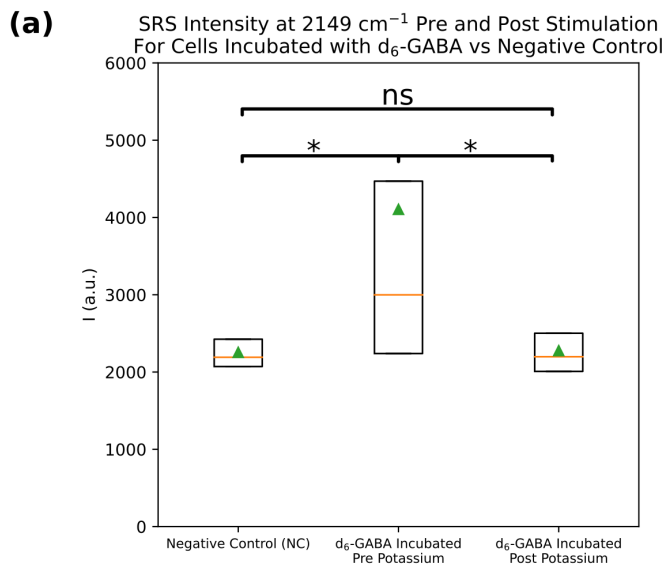
11

hippocampal neurons not incubated with d_6-GABA but otherwise cultured under identical conditions (figure 6, top row). Across many neurons, we observe a significant separation between the average signal intensity in d_6-GABA incubated vs unincubated cells (figure 7a; $p < 0.001$, $\Delta > 5.58$). In contrast to the case of PC12 cells, however, a population of cells do not uptake d_6-GABA, reflected in a substantial overlap between the incubated and unincubated distributions. This large distribution in d_6-GABA uptake is likely due to the many neuronal subtypes that exist in the hippocampus where glutamatergic neurons may be more prevalent than GABAergic neurons (46). Evidence also suggests that glutamine and GABA may coexist and may be co-released in certain neurons, which could affect relative GABA uptake (46, 47). For non-GABAergic, or neurons containing a mixture of multiple neurotransmitters, no or decreased uptake of d_6-GABA is expected.

Fig. 6 SRS imaging of a deuterated GABA isotopologue primary hippocampal neurons.
(a) SRS images of primary hippocampal neurons without incubation with the deuterated GABA

isotopologue (top), with incubation with the GABA isotopologue (middle), and with incubation with the GABA isotopologue, but two minutes post stimulation to release neurotransmitter with 50 mM potassium (bottom). The left column displays images at 2950 cm-1, the C-H stretching frequency range, broadly corresponding to protein signal and allowing cell localization. The right column displays images at 2149 cm-1, the C-D stretching frequency range, corresponding to the signal originating from the deuterated GABA compound.

To examine whether the signal measured at 2149 cm^{-1} did arise from internalized d_6-GABA, we repeated the above dopamine-specific experiments by incubating neurons with 50 μM d_6-GABA for one hour. The neurons were then stimulated with 50 mM potassium. Images were acquired in PBS two minutes after stimulation, after first washing away the potassium and d_6-GABA containing medium. Neurons imaged after potassium stimulation showed little to no observable signal at 2149 cm^{-1} (figure 6, bottom row). This 55% decrease in d_6-GABA signal following potassium stimulation was found to be significant across many cells (figure 7a; $p < 0.001$, $\Delta > 0.65$). When considering that no significant difference was observed between d_6-GABA neurons imaged post potassium stimulation, and unincubated neurons, this result suggests successful and near complete release of internalized d_6-GABA. Together these data suggest the ability to visualize uptake and release of a GABA isotopologue within cultured primary neurons. To the best of our knowledge, these represent the first optical micrographs of the neurotransmitter GABA itself within a a neurobiological system.

(a) SRS Intensity at 2149 cm^{-1} Pre and Post Stimulation For Cells Incubated with d_6-GABA vs Negative Control

Fig. 7 Cell-averaged SRS intensity distributions for cells incubated with deuterated GABA isotopologue.
(a) The cell-averaged SRS intensity for cells that were not incubated with deuterated GABA (left column), cells that were incubated with deuterated GABA (middle column), and cells that were incubated with deuterated GABA, stimulated to release neurotransmitter with 50 mM potassium,

and imaged two minutes later (right column). * $p < 0.001$, $\Delta > 5.58$ (incubated vs negative control), $\Delta > 0.65$ (incubated vs incubated post stimulation). N(negative control) = 1840, N(Incubated, pre-stimulation) = 2110, N(Incubated, post-stimulation) = 2537.

Discussion

Isotopes have long a history of use in neuroscience, which the present report has leveraged and extended to the method of vibrational microscopy. Among the first techniques developed to measure concentrations of neurotransmitters were based on radioactive isotopes (48, 49). Positron emission tomography (PET) continues to make frequent use of radiolabels to study the proteins of the nervous system (50, 51). Powerful mass spectrometry imaging methods use deuterated analogues as calibration standards for quantitative spatial mapping of neurotransmitters (52–54). Herein, we demonstrate that by combining the use of isotopologues with vibrational microscopy, we can to image the biodistribution, and stimulated release, of deuterated dopamine and GABA isotopologues in cultured cells and primary neurons. Our results suggest that commercially-available deuterated neurotransmitters and neuromodulators could be applied to a broad range of studies of neurotransmitter uptake and release kinetics in neuronal cells, tissue, and potentially in living animals. Recent developments in the field of vibrational microscopy also provide opportunities to further enrich the information this technique can provide through integration of orthogonal methodologies that could simultaneously measure neurotransmitter release kinetics and electrical activity, or follow uptake and release of multiple neurotransmitters simultaneously.

SRS microscopy, for instance, has been shown to be sensitive to membrane potential (55), a property recently exploited to track neuron depolarization in response to action potentials (56). In combination with isotopologue imaging, this offers the potential for a single optical system to image both neurochemical and electrical information simultaneously. The narrow linewidths of vibrational transitions (10s cm^{-1}), compared to electronic transitions (100s cm^{-1}), raise the additional possibility of simultaneous observation of multiple neurotransmitters. Acquisition of hyperspectral image stacks, i.e. multiple images of the same field of view at many wavenumbers, allows for the spectral unmixing of the contribution of distinct neurotransmitter isotopologues. A multiplexed imaging strategy could help answer questions surrounding release and uptake of multiple neurotransmitters in single neurons, as in the case of GABA and glutamate, two neurotransmitters that canonically have opposing activity (46, 47).

The current study was limited to cells and primary neurons which could be cultured and prepared for imaging under tight geometric constraints, a consequence of the transmission-based SRS imaging modality. In order to extend the use of neurotransmitter isotopologues to tissue samples, or even live animals, an epi-SRS microscope could be used, with a geometry analogous to more familiar fluorescence-based microscopes. The use of epi-SRS has previously been demonstrated to work in brain tissue (57, 58). In fact, SRS imaging is rather unique in that regard, as signal collection in the epi-direction increases with increasing sample thickness. For samples more than 2 mm thick, it has been found to be preferable to image in this back scattering geometry (59). Additionally, other vibrational imaging techniques are not subject to the same constraints. For instance, CARS, another coherent

14

Raman technique, is frequently implemented in either a transmission or epi geometry, and confocal spontaneous Raman and SERS microscopy are almost exclusively implemented in epi geometries.

Similarly, exclusively intracellular populations of dopamine and GABA were measured using our current imaging setup, since neither spontaneous Raman nor SRS microscopy are likely to achieve the sensitivity required to observe the lower concentrations of neurotransmitter present extracellularly. For neuromodulators like dopamine, for which the study of volume transmission is of interest, their extracellular concentrations can vary widely but are often present at 20 nM concentrations extracellularly (60). Isotopologue imaging for intracellular studies combined with existing probes to image volume transmission would present a powerful apporach to track neurotransmitter uptake, release, and volume transmission. As such, the current combination of neurotransmitter isotopologues and SRS microscopy is best implemented to study intracellular neurotransmitter populations and can serve as an orthogonal measure, complementing other tools available to study neuromodulator volume transmission. These include direct extracellular concentration sensors, such as those based on carbon nanotubes or genetically engineered proteins, or techniques like magnetic resonance spectroscopic imaging (MRSI), which is used to study neurotransmitter concentrations under a variety of paradigms. While powerful, MRSI is unable to distinguish intracellular and extracellular contributions to the signal (61), due to lower spatiotemporal resolution, a void which this technique may help to fill when questions of mechanism or attribution arise. Additionally signal enhancement techniques may also be used to further increase the sensitivity of vibrational microscopy. Recent work suggests that surface enhanced SRS (SESRS) can be used to image at the single molecule level under certain conditions, as demonstrated with bacterial cells in (62). Similar observations have been made for surface enhanced CARS (SECARS) (63–65). Furthermore, a recent study (66)describes a widefield implementation of SECARS which could extend that level of sensitivity to the ms temporal resolution of more conventional widefield microscopies. While the use of plasmonic nanoparticles, or culturing on plasmonic nanostructure surfaces, introduces an additional level of complexity, the SERS field has frequently demonstrated its applicability to and utility in neuroimaging (67, 68), even in intraoperative/clinical settings (69, 70).

In this report we have presented a practical strategy to image neurotransmitters under native biological conditions using vibrational microscopy. This strategy generalizes to any class of neurotransmitter, many of which are already commercially available in isotope-labeled form, opening new avenues for fundamental investigations into the biology of neurotransmitters. Notably, many commericially-available isotopologes, such as GABA as demonstrated here, are neurotransmitters or neuromodulators that lack cellular-scale imaging tools. While this work represents the first demonstration of the use of isotopologues and vibrational microscopy in this context, it makes use of a technique, i.e. isotope labeling, which is broadly familiar to both the microscopy and neuroscience communities. Furthermore, a growing demand for new tools to study the nervous system has led to increasing adoption of vibrational imaging methods in neuroscience, and a focus on adapting existing imaging techniques to tackle the unique problems that poses in the imaging community. As such, this positions this strategy as a tool with the potential for wide adoption to further the understanding of neurotransmission.

Materials and Methods

PC12 cell culture

PC12 rat chromaffin cells (UC Berkeley cell culture facillity) were continuously cultured in RPMI-1640 medium with L-glutamine, containing 10% goat serum, 10% FBS, and 1% penicillin/streptomycin. For d4-DA imaging, cells were passaged onto 25 mm diameter round coverslips. For FFN102 imaging, cells were passaged into 24 well-plates. Upon achieving 50-70% confluency on the coverslips, the media was exchanged to a serum deprived DMEM media, containing 0.5% FBS, 1% penicillin/streptomycin, and 100 ng/mL NGF-β. The coverslips were imaged 5 days post media exchange. The cells were maintained in an incubator at 37 °C and 5% CO2.

Flow cell construction and PC12 cell culture on device

A consequence of the chosen imaging modality for d4-DA is a set of strict geometric constraints for sample placement on the microscope. This is due to the fact that the SRS signal is, generally, collected in a transmission geometry, requiring the sample be placed between an objective and collecting lens. SRS microscopy can also be subject to non-specific signals arising from the optical Kerr effect in the form of cross-phase modulation (XPM). The most straight-forward way to reduce or eliminate this effect is to use a collecting lens with a numerical aperture equal to or larger than that of the objective lens (71), necessitating a 1.4 NA oil immersion condenser lens, for use with the 1.2 NA water immersion objective used in this study. Introduction of potassium, for the stimulation of a sample that has just been imaged, is complicated by the presence of these two immersion fluids, and the need to keep the sample sealed off from both. In order to make measurements of d4-DA signal intensity on the same PC12 cells both before and after potassium stimulation we constructed a simple flow cell.

The flow cell was constructed using two 48 x 60 mm coverslips (Gold Seal, Thermo scientific). RTV 615 PDMS was first mixed in a 10:1 ratio of monomer to cross-linker. PEEK tubing (1/32"x0.010, IDEX Health and Science) was cut into lengths of 2" to serve as inlets into the device, and to control the height of the device. Two lengths of tubing were placed in the center of one short edge of the coverslip, while another two were placed along the entire length of each long edge. The PDMS mixture was then applied using a brush along the two long edges and the short edge with tube inlets. The PDMS was applied in a thickness equal to the height of the PEEK tubing extending up from the coverslip. The second coverslip was then placed on top, enclosing the device. The device was baked for 10 minutes at 70 °C, then flushed with ethanol and further sterilized under UV-C light for 2 minutes. The final height of the devices was 1.1 mm.

PC12 cells were introduced to the device by extracting 2 mL of trypsanized cells from the passaging culture using a syringe, sterilized as above using ethanol and UV-C light, and then affixing the syringe to one of the available inlets. Cells were allowed to grow for 2 days before the medium was exchanged for the serum deprived medium. Cells were grown for a further 5 days before imaging, the same as those on coverslips. The devices were maintained within separate sterile petri dishes in the same incubator until imaging.

Primary hippocampal neuron dissociation and culture

Neurons were dissociated from extracted hippocampi of day 19 embryos of Sprague Dawley rats, as previously described (72). Briefly, cells are dissociated for 15 minutes from excised hippocampi using a trypsinated buffer. The neurons are then plated onto 25 mm coverslips and incubated at 37 °C in MEM medium with 5% FBS, 2% B-27, 2% 1M dextrose and 1% GlutaMax. One day after dissociation, half the medium is exchanged for neurobasal medium with 2% B-27 supplement and 1% GlutaMax, to prevent proliferation of glial cells. Coverslips are then imaged using SRS microscopy two weeks post dissociation.

SRS microscope optical setup

The optical setup has been described previously (73)and is shown in figure S2. Briefly, the synchronized dual output from a commercial femtosecond laser/OPO system is used for the pump and Stokes beams. The Stokes beam was fixed at 1040 nm, while the pump was tunable. For imaging at 2950 cm^{-1}, 2149 cm^{-1}, and 2135 cm^{-1}, the pump was tuned to 796 nm, 850 nm, and 851 nm respectively. The Stokes beam was intensity modulated at 10.28 MHz using a quarter waveplate (Thorlabs), a resonant electro-optic modulator (Thorlabs), driven by a function generator (Hewlett Packard) and power amplifier (Minicircuits), and a polarizer (Thorlabs). The pump and stokes were combined colinearly using a 1000 nm short pass dichroic mirror. Temporal coincidence of the pulses was controlled using an optical delay line (Newport). A commercial scanning microscope (FV1200, Olympus) was used to raster scan the beams across the sample. A 60x 1.2 NA water immersion objective (Olympus) was used for excitation, and a 1.4 NA oil immersion condenser (Thorlabs) was used to collect the transmitted light. The Stokes beam was filtered by a 1000 nm shortpass filter, before the pump was detected on a photodiode (Hamatasu) reverse biased at 61.425. The stimulated Raman loss signal was extracted from the photodiode signal using a lock-in amplifier (Zurich Instruments).

Deuterated neurotransmitter imaging

PC12 cells or primary neurons cultured on coverslips were incubated for one hour at 37 °C with a final media concentration of 50 μM d4-DA or d6-GABA, respectively. After one hour the coverslips were washed three times with DPBS, before being placed on 25 mm diameter, low-profile 600 μm culture dish (Grace coverwells), filled with DPBS. The edges of the culture dish contain an adherent which fixed the coverslips in place. PC12 cells were then imaged at 2950 cm^{-1} and 2135 cm^{-1} using the SRS microscope. The pump and Stokes power were both set to 20 mW. Images were acquired at a size of 512 x 512 pixels, using a 10 μs pixel dwell time and a lock-in constant of 3 μs. Neurons were imaged using a pump and Stokes power of 15 mW, and at 2950 cm^{-1} and 2149 cm^{-1}, but otherwise identical imaging conditions. For the negative control samples for both PC12 cells and primary neurons, the media was exchanged for fresh media not containing the deuterated compound. The cells were then left to rest for one hour before being washed three times with DPBS and prepared identically to the cells incubated with the deuterated isotopologues, and imaged using the same conditions. For the post stimulation condition PC12 cells and primary neurons were incubated with 50

μM d4-DA or d6-GABA, respectively. After a one hour incubation, the media was exchanged for media containing 50 mM potassium. After two minutes, the coverslips were washed twice with DPBS, and prepared and imaged analogously to the previously described conditions.

PC12 cells which were cultured on the flow cell devices were incubated with 50 μM d4-DA by first emptying the device of media through the open side and then introducing new media with the deuterated compound. After one hour the device was then washed twice with DPBS, before being filled with fresh media. In contrast to the PC12 cells cultured on coverslips, those cultured on the device were imaged in media not DPBS, in order to enable stimulated release of the d4-DA while on the microscope. The devices were then imaged with the same settings as those used for the cells cultured on coverslips. One image was taken at 2950 cm^{-1}, then a pre stimulation image at 2135 cm^{-1}, an image at 2135 cm^{-1} following influx of media not containing supplemental potassium, and finally a post-stimulation image 2 minutes after an influx of 50 mM potassium. This set of images was also repeated for PC12 cells cultured on devices which were not incubated with d4-DA.

Two-photon excited fluorescence imaging of FFN102

For imaging of FFN fluorescence in PC12 cells, the cells were first incubated to a final media concentration of 10 μM FFN102 for one hour at 37 °C. After one hour, samples were washed three times with DPBS. For imaging, the pump wavelength on the SRS microscope was tuned to 800 nm for two-photon excitation of FFN102, with the power set to 20 mW. Images were acquired in the epi-direction at a size of 512 x 512 pixels, using a 10 μs pixel dwell time and non-descan PMT available on the Olympus microscope. For post potassium stimulation measurements, FFN102 was either imaged in cells 2 minutes after exposure to potassium in adjacent wells on the well plate that had not been previously imaged, or for measurements on the same cells, 2 minutes after exposure to potassium in a well that had been previously imaged.

Image processing

All statistics reported are calculated over the intensity distribution of the average signal in individual cells. Statistical significance was tested using a Welch's T-test assuming unequal variance. Effect sizes are displayed as Glass' Δ. For calculations involving SRS images, all images in both the 2950 cm^{-1} and 2135 cm^{-1} or 2149 cm^{-1} are pseudo-flatfield corrected using a replica of the respective image, convolved with Gaussian kernel of radius 200 pixels, as the flatfield. The 2950 cm^{-1} channel images are then used for thresholding and segmentation. First a Gaussian blur of radius 5 pxiels is applied, followed by a contrast limited adaptive histogram equilization with of radius 15. Otsu's method is then applied to produce a binary thresholded image. A hierarchical contour tracing algorithm is then used to determine the outlines of the thresholded image. Internal contours, arising from organelles or low-intensity regions within a cell, are discarded, leaving the highest level outlines of the cell. Any contours with a total length of less than 100 pixels are also discarded. Each of the remaining contours is used to determine a mask over which the signal inside the contour is averaged in the corresponding 2135 cm^{-1} or 2149 cm^{-1} channel. Beyond flatfield corrections the channels corresponding to deuterated compounds undergo no additional processing.

Fluorescence images of PC12 cells incubated with FFN102 are processed similarly; however, as the signal is strong enough to see cell boundaries in the fluorescence channel, no additional channel is needed to serve as the mask. Instead, after flatfield correction, a second copy of each image is used for masking, and undergoes the same processing as the SRS images acquired in the 2950 cm^{-1}. The discovered contours are then used as masks on the unprocessed copy.

Acknowledgements

Funding

References

1. T. C. Südhof, The Synaptic Vesicle Cycle. Annu. Rev. Neurosci. 27, 509–547 (2004).

2. C. Grienberger, A. Konnerth, Imaging Calcium in Neurons. Neuron. 73, 862–885 (2012).

3. J. P. Kesby, D. W. Eyles, J. J. McGrath, J. G. Scott, Dopamine, psychosis and schizophrenia: The widening gap between basic and clinical neuroscience. Transl. Psychiatry. 8 (2018), doi:10.1038/s41398-017-0071-9.

4. M. S. Starr, The Role of Dopamine in Epilepsy. Synapse. 22, 159–194 (1996).

5. N. Warren, C. O'Gorman, A. Lehn, D. Siskind, Dopamine dysregulation syndrome in Parkinson's disease: A systematic review of published cases. J. Neurol. Neurosurg. Psychiatry. 88, 1060–1064 (2017).

6. J. Y. Chen, E. A. Wang, C. Cepeda, M. S. Levine, Dopamine imbalance in Huntington's disease: A mechanism for the lack of behavioral flexibility. Front. Neurosci. 7, 1–14 (2013).

7. D. J. Nutt, A. Lingford-Hughes, D. Erritzoe, P. R. A. Stokes, The dopamine theory of addiction: 40 years of highs and lows. Nat. Rev. Neurosci. 16, 305–312 (2015).

8. W. J. Betz, F. Mao, G. S. Bewick, Activity-dependent fluorescent staining and destaining of living vertebrate motor nerve terminals. J. Neurosci. 12, 363–375 (1992).

9. S. Sankaranarayanan, D. De Angelis, J. E. Rothman, T. A. Ryan, The use of pHluorins for optical measurements of presynaptic activity. Biophys. J. 79, 2199–2208 (2000).

10. E. Lacin, A. Muller, M. Fernando, D. Kleinfeld, P. A. Slesinger, Construction of Cell-based Neurotransmitter Fluorescent Engineered Reporters (CNiFERs) for Optical Detection of Neurotransmitters In Vivo. J. Vis. Exp., 1–13 (2016).

11. D. A. Arroyo, L. A. Kirkby, M. B. Feller, Retinal Waves Modulate an Intraretinal Circuit of Intrinsically Photosensitive Retinal Ganglion Cells. J. Neurosci. 36, 6892–6905 (2016).

12. F. Sun, J. Zeng, M. Jing, J. Zhou, J. Feng, F. Owen, Y. Luo, F. Li, H. Wang, T. Yamaguchi, Z. Yong, Y. Gao, W. Peng, L. Wang, S. Zhang, J. Du, D. Lin, A. C. Kreitzer, G. Cui, Y. Li, A genetically-encoded fluorescent sensor enables rapid and specific detection of dopamine in flies, fish, and mice. Cell. 174, 481–496 (2018).

13. T. Patriarchi, J. R. Cho, K. Merten, M. W. Howe, A. Marley, W. Xiong, R. W. Folk, G. J. Broussard, R. Liang, M. J. Jang, H. Zhong, D. Dombeck, M. Von Zastrow, A. Nimmerjahn, V. Gradinaru, J. T. Williams, L. Tian, Ultrafast neuronal imaging of dopamine dynamics with designed genetically encoded sensors. Science (80-.). 360 (2018).

14. S. Kruss, D. P. Salem, L. Vukovi, B. Lima, E. Vander Ende, E. S. Boyden, M. S. Strano, High-resolution imaging of cellular dopamine efflux using a fluorescent nanosensor array. PNAS. 3 (2017), doi:10.1073/pnas.1613541114.

15. A. G. Beyene, K. Delevich, J. Travis, D. B. Donnell, D. J. Piekarski, W. C. Lin, A. W. Thomas, S. J. Yang, P. Kosillo, D. Yang, G. S. Prounis, L. Wilbrecht, M. P. Landry, Imaging striatal dopamine release using a nongenetically encoded near infrared fluorescent catecholamine nanosensor. Sci. Adv. 5 (2019).

16. C. Bulumulla, A. T. Krasley, D. Walpita, A. G. Beyene, bioRxiv, in press.

17. P. C. Rodriguez, D. B. Pereira, A. Borgkvist, M. Y. Wong, C. Barnard, M. S. Sonders, H. Zhang, D. Sames, D. Sulzer, Fluorescent dopamine tracer resolves individual dopaminergic synapses and their activity in the brain. Proc. Natl. Acad. Sci. U. S. A. 110, 870–875 (2013).

18. D. B. Pereira, Y. Shmitz, J. Mészáros, P. Merchant, G. Hu, S. Li, A. Henke, J. E. Lizardi-Ortiz, R. J. Karpowicz Jr, T. J. Morgenstern, M. S. Sonders, E. Kanter, P. C. Rodriguez, E. V. Mosharov, D. Sames, D. Sulzer, Fluorescent false neurotransmitter reveals functionally silent dopamine vesicle clusters in the striatum. Nat. Neurosci. 19, 578–586 (2016).

19. A. Henke, Y. Kovalyova, M. Dunn, D. Dreier, N. G. Gubernator, I. Dincheva, C. Hwu, P. Šebej, M. S. Ansorge, D. Sulzer, D. Sames, Toward Serotonin Fluorescent False Neurotransmitters: Development of Fluorescent Dual Serotonin and Vesicular Monoamine Transporter Substrates for Visualizing Serotonin Neurons. ACS Chem. Neurosci. 9, 925–934 (2018).

20. J. Balaji, R. Desai, S. K. Kaushalya, M. J. Eaton, S. Maiti, Quantitative measurement of serotonin

synthesis and sequestration in individual live neuronal cells. J. Neurochem. 95, 1217–1226 (2005).

21. B. K. Maity, S. Maiti, Label-free imaging of neurotransmitters in live brain tissue by multi-photon ultraviolet microscopy. Neuronal Signal. 2, 1–14 (2018).

22. B. Sarkar, A. Banerjee, A. K. Das, S. Nag, S. K. Kaushalya, U. Tripathy, M. Shameem, S. Shukla, S. Maiti, Label-Free Dopamine Imaging in Live Rat Brain Slices. ACS Chem. Neurosci. 5, 329–334 (2014).

23. D. Fu, W. Yang, X. S. Xie, Label-free imaging of neurotransmitter acetylcholine at neuromuscular junctions with stimulated Raman scattering. J. Am. Chem. Soc. 139, 583–586 (2017).

24. H. Yamakoshi, K. Dodo, M. Okada, J. Ando, A. Palonpon, K. Fujita, S. Kawata, M. Sodeoka, Imaging of EdU, an alkyne-tagged cell proliferation probe, by Raman microscopy. J. Am. Chem. Soc. 133, 6102–6105 (2011).

25. L. Wei, F. Hu, Y. Shen, Z. Chen, Y. Yu, C. C. Lin, M. C. Wang, W. Min, Live-cell imaging of alkyne-tagged small biomolecules by stimulated Raman scattering. Nat. Methods. 11, 410–412 (2014).

26. H. Yamakoshi, A. Palonpon, K. Dodo, J. Ando, S. Kawata, K. Fujita, M. Sodeoka, A sensitive and specific Raman probe based on bisarylbutadiyne for live cell imaging of mitochondria. Bioorganic Med. Chem. Lett. 25, 664–667 (2015).

27. F. Hu, C. Zeng, R. Long, Y. Miao, L. Wei, Q. Xu, W. Min, Supermultiplexed optical imaging and barcoding with engineered polyynes. Nat. Publ. Gr. (2018), doi:10.1038/nmeth.4578.

28. Z. Zhao, Y. Shen, F. Hu, W. Min, Applications of vibrational tags in biological imaging by Raman microscopy. Analyst, 4018–4029 (2017).

29. M. Nuriya, Y. Ashikari, T. Iino, T. Asai, J. Shou, K. Karasawa, K. Nakamura, Y. Ozeki, Y. Fujimoto, M. Yasui, Alkyne-Tagged Dopamines as Versatile Analogue Probes for Dopaminergic System Analysis. Anal. Chem. 93, 9345–9355 (2021).

30. A. Alfonso-García, S. G. Pfisterer, H. Riezman, E. Ikonen, E. O. Potma, D38-cholesterol as a Raman active probe for imaging intracellular cholesterol storage. J. Biomed. Opt. 21, 061003 (2015).

31. Y. Shen, F. Xu, L. Wei, F. Hu, W. Min, Live-cell quantitative imaging of proteome degradation by stimulated raman scattering. Angew. Chemie - Int. Ed. 53, 5596–5599 (2014).

32. L. Shi, C. Zheng, Y. Shen, Z. Chen, E. S. Silveira, L. Zhang, M. Wei, C. Liu, C. de Sena-Tomas, K. Targoff, W. Min, Optical imaging of metabolic dynamics in animals. Nat. Commun. 9 (2018), doi:10.1038/s41467-018-05401-3.

33. C. W. Freudiger, W. Min, B. G. Saar, S. Lu, G. R. Holtom, C. He, J. C. Tsai, J. X. Kang, S. X. Xie, Label-Free Biomedical Imaging with High Sensitivity by Stimulated Raman Scattering Microscopy. Science (80-.). 322, 1857–1861 (2008).

34. D. W. McCamant, P. Kukura, R. A. Mathies, Femtosecond Broadband Stimulated Raman: A New Approach for High-Performance Vibrational Spectroscopy. Appl. Spectrosc. 57, 1317–1323 (2003).

35. R. H. S. Westerink, A. G. Ewing, The PC12 cell as model for neurosecretion. Acta Physiol. 192, 273–285 (2008).

36. S. R. Jones, J. D. Joseph, L. S. Barak, M. G. Caron, R. M. Wightman, Dopamine neuronal transport kinetics and effects of amphetamine. J. Neurochem. 73, 2406–2414 (1999).

37. T. M. Olefirowicz, A. G. Ewing, Dopamine concentration in the cytoplasmic compartment of single neurons determined by capillary electrophoresis. J. Neurosci. Methods. 34, 11–15 (1990).

38. T. K. Chen, G. Luo, A. G. Ewing, Amperometric Monitoring of Stimulated Catecholamine Release from Rat Pheochromocytoma (PC12) Cells at the Zeptomole Level. Anal. Chem. 66, 3031–3035 (1994).

39. R. M. Wightman, J. A. Jankowski, R. T. Kennedy, K. T. Kawagoe, T. J. Schroeder, D. J. Leszczyszyn, J. A. Near, E. J. Diliberto, O. H. Viveros, Temporally resolved catecholamine spikes correspond to single vesicle release from individual chromaffin cells. Proc. Natl. Acad. Sci. U. S. A. 88 (1991), pp. 10754–10758.

40. R. H. S. Westerink, A. De Groot, H. P. M. Vijverberg, Heterogeneity of catecholamine-containing vesicles in PC12 cells. Biochem. Biophys. Res. Commun. 270, 625–630 (2000).

41. N. Lecat-Guillet, C. Monnier, X. Rovira, J. Kniazeff, L. Lamarque, J. M. Zwier, E. Trinquet, J. P. Pin, P. Rondard, FRET-Based Sensors Unravel Activation and Allosteric Modulation of the GABA B Receptor. Cell Chem. Biol. 24, 360–370 (2017).

42. A. Masharina, L. Reymond, D. Maurel, K. Umezawa, K. Johnsson, A fluorescent sensor for GABA and synthetic GABAB receptor ligands. J. Am. Chem. Soc. 134, 19026–19034 (2012).

43. J. S. Marvin, Y. Shimoda, V. Magloire, M. Leite, T. Kawashima, T. P. Jensen, I. Kolb, E. L. Knott, O. Novak, K. Podgorski, N. J. Leidenheimer, D. A. Rusakov, M. B. Ahrens, D. M. Kullmann, L. L. Looger, A genetically encoded fluorescent sensor for in vivo imaging of GABA. Nat. Methods. 16, 763–770 (2019).

44. D. L. Rothman, O. A. C. Petroff, K. L. Behar, R. H. Mattson, Localized 1H NMR measurements of γ-aminobutyric acid in human brain in vivo. Proc. Natl. Acad. Sci. U. S. A. 90, 5662–5666 (1993).

45. Y. Wu, W. Wang, A. Díez-Sampedro, G. B. Richerson, Nonvesicular Inhibitory Neurotransmission via Reversal of the GABA Transporter GAT-1. Neuron. 56, 851–865 (2007).

46. H. Zhu, G. Zou, N. Wang, M. Zhuang, W. Xiong, G. Huang, Single-neuron identification of chemical constituents, physiological changes, and metabolism using mass spectrometry. Proc. Natl. Acad. Sci. U. S. A. 114, 2586–2591 (2017).

47. S. J. Shabel, C. D. Proulx, J. Piriz, R. Malinow, GABA/glutamate co-release controls habenula output and is modified by antidepressant treatment. Science (80-.). 345, 1494–1498 (2014).

48. J. M. Bowdler, A. R. Green, M. C. W. Minchin, D. J. Nutt, Regional GABA concentration and [3H]-diazepam binding in rat brain following repeated electroconvulsive shock. J. Neural Transm. 56, 3–12 (1983).

49. L. M. Lieberman, W. H. Beierwaltes, V. M. Varma, P. Weinhold, R. Ling, Labeled dopamine concentration in human adrenal medulla and in neuroblastoma. J. Nucl. Med. 10, 93–97 (1969).

50. X. Chen, T. Kudo, C. Lapa, A. Buck, T. Higuchi, Recent advances in radiotracers targeting norepinephrine transporter: structural development and radiolabeling improvements. J. Neural Transm. 127, 851–873 (2020).

51. J. S. Stehouwer, M. M. Goodman, Fluorine-18 Radiolabeled PET Tracers for Imaging Monoamine Transporters: Dopamine, Serotonin, and Norepinephrine. PET Clin. 4, 101–128 (2009).

52. A. M. A. P. Fernandes, P. H. Vendramini, R. Galaverna, N. V. Schwab, L. C. Alberici, R. Augusti, R. F. Castilho, M. N. Eberlin, Direct Visualization of Neurotransmitters in Rat Brain Slices by Desorption Electrospray Ionization Mass Spectrometry Imaging (DESI - MS). J. Am. Soc. Mass Spectrom. 27,

1944–1951 (2016).

53. M. Shariatgorji, A. Nilsson, R. J. A. Goodwin, P. Källback, N. Schintu, X. Zhang, A. R. Crossman, E. Bezard, P. Svenningsson, P. E. Andren, Direct targeted quantitative molecular imaging of neurotransmitters in brain tissue sections. Neuron. 84, 697–707 (2014).

54. K. Y. Zhu, Q. Fu, K. W. Leung, Z. C. F. Wong, R. C. Y. Choi, K. W. K. Tsim, The establishment of a sensitive method in determining different neurotransmitters simultaneously in rat brains by using liquid chromatography-electrospray tandem mass spectrometry. J. Chromatogr. B Anal. Technol. Biomed. Life Sci. 879, 737–742 (2011).

55. B. Liu, H. J. Lee, D. Zhang, C. S. Liao, N. Ji, Y. Xia, J. X. Cheng, Label-free spectroscopic detection of membrane potential using stimulated Raman scattering. Appl. Phys. Lett. 106 (2015), doi:10.1063/1.4919104.

56. H. J. Lee, D. Zhang, Y. Jiang, X. Wu, P. Y. Shih, C. S. Liao, B. Bungart, X. M. Xu, R. Drenan, E. Bartlett, J. X. Cheng, Label-Free Vibrational Spectroscopic Imaging of Neuronal Membrane Potential. J. Phys. Chem. Lett. 8, 1932–1936 (2017).

57. K. Bae, W. Zheng, K. Lin, S. W. Lim, Y. K. Chong, C. Tang, N. K. King, C. B. Ti Ang, Z. Huang, Epi-Detected Hyperspectral Stimulated Raman Scattering Microscopy for Label-Free Molecular Subtyping of Glioblastomas. Anal. Chem. 90, 10249–10255 (2018).

58. M. Ji, D. A. Orringer, C. W. Freudiger, S. Ramkissoon, X. Liu, D. Lau, A. J. Golby, I. Norton, M. Hayashi, N. Y. R. Agar, G. S. Young, C. Spino, S. Santagata, S. Camelo-Piragua, K. L. Ligon, O. Sagher, X. S. Xie, Rapid, Label-Free Detection of Brain Tumors with Stimulated Raman Scattering Microscopy. Sci. Transl. Med. 5 (2013).

59. A. H. Hill, B. Manifold, D. Fu, Tissue imaging depth limit of stimulated Raman scattering microscopy. Biomed. Opt. Express. 11, 762 (2020).

60. C. J. Watson, B. J. Venton, R. T. Kennedy, In vivo measurements of neurotransmitters by microdialysis sampling. Anal. Chem. 78, 1391–1399 (2006).

61. B. Spurny, R. Seiger, P. Moser, T. Vanicek, M. B. Reed, E. Heckova, P. Michenthaler, A. Basaran, G. Gryglewski, M. Klöbl, S. Trattnig, S. Kasper, W. Bogner, R. Lanzenberger, Hippocampal GABA levels correlate with retrieval performance in an associative learning paradigm. Neuroimage. 204 (2020), doi:10.1016/j.neuroimage.2019.116244.

62. C. Zong, R. Premasiri, H. Lin, Y. Huang, C. Zhang, C. Yang, B. Ren, L. D. Ziegler, J. X. Cheng, Plasmon-enhanced stimulated Raman scattering microscopy with single-molecule detection sensitivity. Nat. Commun. 10, 1–11 (2019).

63. T.-W. Koo, S. Chan, A. A. Berlin, Single-molecule detection of biomolecules by surface-enhanced coherent anti-Stokes Raman scattering. Opt. Lett. 30, 1024 (2005).

64. C. Steuwe, C. F. Kaminski, J. J. Baumberg, S. Mahajan, Surface enhanced coherent anti-stokes raman scattering on nanostructured gold surfaces. Nano Lett. 11, 5339–5343 (2011).

65. Y. Zhang, Y. R. Zhen, O. Neumann, J. K. Day, P. Nordlander, N. J. Halas, Coherent anti-Stokes Raman scattering with single-molecule sensitivity using a plasmonic Fano resonance. Nat. Commun. 5, 1–7 (2014).

66. C. Zong, R. Cheng, F. Chen, P. Lin, M. Zhang, Z. Chen, C. Li, C. Yang, J. X. Cheng, Wide-Field Surface-Enhanced Coherent Anti-Stokes Raman Scattering Microscopy. ACS Photonics (2021), doi:10.1021/acsphotonics.1c02015.

67. R. J. Diaz, P. Z. McVeigh, M. A. O'Reilly, K. Burrell, M. Bebenek, C. Smith, A. B. Etame, G. Zadeh, K. Hynynen, B. C. Wilson, J. T. Rutka, Focused ultrasound delivery of Raman nanoparticles across the blood-brain barrier: Potential for targeting experimental brain tumors. Nanomedicine Nanotechnology, Biol. Med. 10, 1075–1087 (2014).

68. F. Nicolson, B. Andreiuk, C. Andreou, H. T. Hsu, S. Rudder, M. F. Kircher, Non-invasive in vivo imaging of cancer using Surface-Enhanced spatially offset raman spectroscopy (SESORS). Theranostics. 9, 5899–5913 (2019).

69. H. Karabeber, R. Huang, P. Iacono, J. M. Samii, K. Pitter, E. C. Holland, M. F. Kircher, Guiding brain tumor resection using surface-enhanced Raman scattering nanoparticles and a hand-held Raman scanner. ACS Nano. 8, 9755–9766 (2014).

70. C. Jiang, Y. Wang, W. Song, L. Lu, Delineating the tumor margin with intraoperative surface-enhanced Raman spectroscopy. Anal. Bioanal. Chem. 411, 3993–4006 (2019).

71. P. Berto, E. R. Andresen, H. Rigneault, Background-free stimulated raman spectroscopy and microscopy. Phys. Rev. Lett. 112, 1–5 (2014).

72. G. Ortiz, P. Liu, P. E. Deal, A. K. Nensel, K. N. Martinez, K. Shamardani, H. Adesnik, E. W. Miller, A silicon-rhodamine chemical-genetic hybrid for far red voltage imaging from defined neurons in brain slice. RSC Chem. Biol. 2, 1594–1599 (2021).

73. S. Kim, G. Dorlhiac, R. Cotrim Chaves, M. Zalavadia, A. Streets, Paper-thin multilayer microfluidic devices with integrated valves. Lab Chip. 21, 1287–1298 (2021).

Supplementary Material
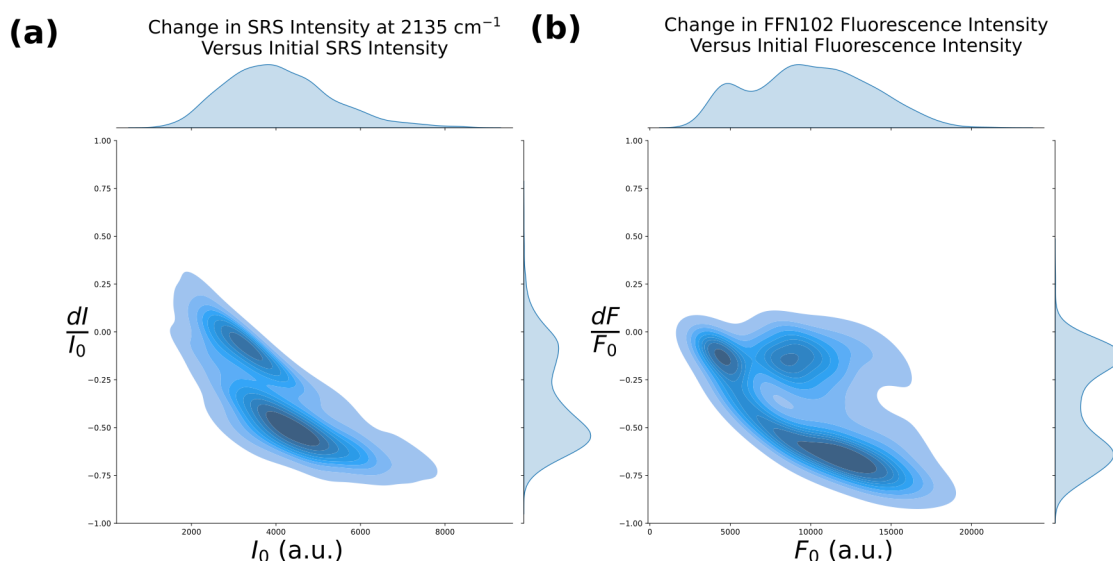
Fig. S1 Relative intensity change of d_4-DA and FFN102 due to potassium stimulation versus initial intensity.

(a) The two-dimensional histogram displaying the relative change in SRS intensity of d_4-DA at 2135 cm^{-1} due to potassium stimulation, versus the initial SRS intensity at 2135 cm^{-1} per cell. The one-dimensional histograms for the relative change distribution, and initial intensity distribution, are displayed on the right and top axes, respectively. The distribution on the right axis corresponds to the violin plot depicted in figure 4b. (b) The corresponding two-dimensional histogram for the relative change in FFN102 fluorescence intensity due to potassium stimulation versus the initial fluorescence intensity per cell. The one-dimensional histogram on the right axis corresponds to the violin plot in figure 4c. There is an additional third population of cells among those incubated with FFN102, not present in the PC12 cells incubated with d_4-DA, which display an high initial fluorescence intensity but little to no change in intensity in response to potassium stimulation.
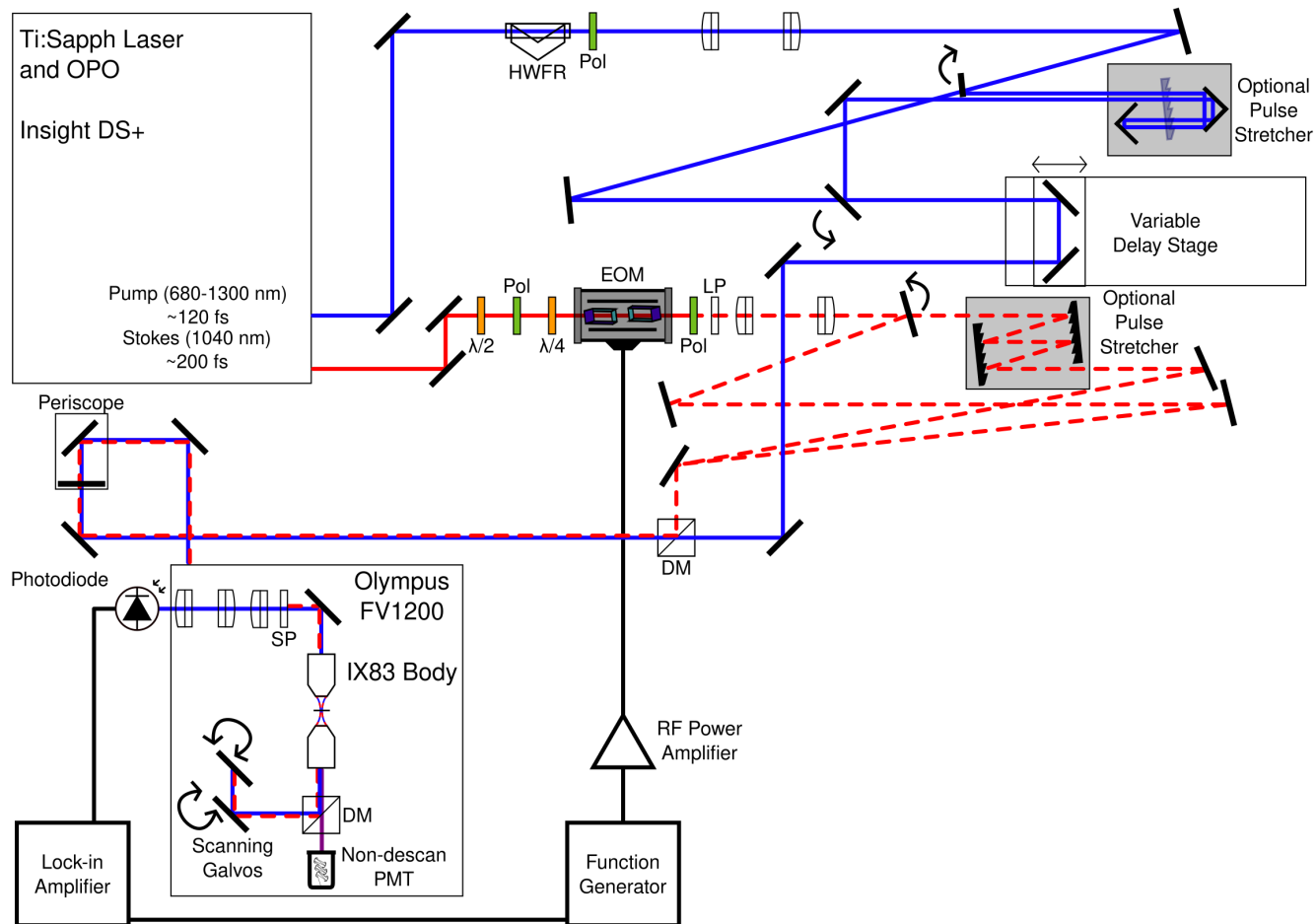
Fig. S2 Schematic of optical setup.
Solid black lines represent mirrors, black lines with ridges are reflective gratings, with the translucent variant being a transmission grating. Lenses are doublets depicted as unlabeled white components outlined in black. EOM: Electro-optic modulator; $\lambda/2$: half-wave plate; Pol: polarizer; $\lambda/4$: quarter-wave plate; LP: long-pass filter; DM: dichroic mirror; SP: short-pass filter.